800 nm WDM Interrogation System for Strain, Temperature, and Refractive Index Sensing Based on Tilted Fiber Bragg Grating

Rui Suo, Xianfeng Chen, Kaiming Zhou, Lin Zhang, and Ian Bennion, *Member, IEEE*

***Abstract*—A low-cost high-resolution wavelength-division-multiplexing (WDM) interrogation system operating around 800 nm region with operational bandwidth up to 60 nm and resolution of 12.7 pm utilizing a tilted fiber Bragg grating (TFBG) and a CCD-array detector has been implemented. The system has been evaluated for interrogating fiber Bragg grating based strain, temperature sensors, giving sensitivities of 0.59 $\mathrm{pm}/\mu\varepsilon$ and 5.6 $\mathrm{pm}/^{\circ}\mathrm{C}$, which are in good agreement with previously reported values. Furthermore, the system has been utilized to detect the refractive index change of sample liquids, demonstrating a capability of measuring index change as small as 10^{-5}. In addition, the vectorial expression of phase match condition and fabrication of TFBG have been discussed.**

***Index Terms*—Optical sensing, strain and temperature sensor, tilted fiber Bragg grating (TFBG), wavelength-division-multiplexing (WDM) interrogation system.**

I. Introduction

FROM THE earliest stage of their development, fiber Bragg gratings (FBGs) have been considered as excellent sensor elements, suitable for measuring static and dynamic fields, such as temperature, strain, and pressure [1]. Due to their advantages of linearity, very low insertion loss, immune to the electromagnetic interference, small size, and easily being embedded in materials, FBGs become compatible with applications in high radiation environment, in the human body for temperature profiling and in composite-embedding for local damage detection, offering the promise of real-time structural measurements.

Tilted fiber Bragg gratings (TFBGs) consist of periodic perturbation to the refractive index of the fiber just as normal Bragg gratings but with tilted fringes (Fig. 1). TFBGs were previously shown to have the ability to couple light out of the fiber core in a certain wavelength range and thus introduce high attenuation to the bounded core modes at these wavelengths [2]. Since the first report as optical taps [3], TFBGs have been used in interrogation systems as spectrometers [4]–[8]. The TFBG used in most reported work, so far, are with responses around 1300 or 1550 nm. However, in some applications, such as medical optics, spectral region around 800 nm is more often used.

Manuscript received August 30, 2007; revised December 13, 2007; accepted December 13, 2007. Published July 16, 2008 (projected). This work was supported in part by the U.K. Overseas Research Students Awards Scheme. The associate editor coordinating the review of this paper and approving it for publication was Prof. Ignacio Matias.

The authors are with the Photonics Research Group, Aston University, Aston Triangle, Birmingham, B4 7ET, U.K. (e-mail address: suor@aston.ac.uk; chenx2@aston.ac.uk; k.zhou@aston.ac.uk; l.zhang@aston.ac.uk; i.bennion@aston.ac.uk).

Digital Object Identifier 10.1109/JSEN.2008.926527

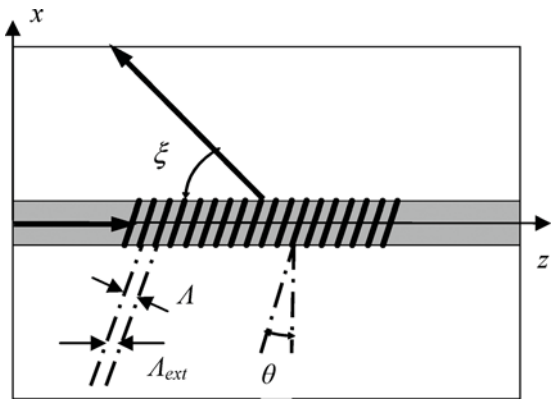

Fig. 1. A schematic diagram showing the structure of a tilted fiber Bragg grating with a given period in a step index optical fiber.

Also, devices such as CCD array detectors and light emitting diodes (LEDs) working in this spectral region are usually much cheaper than those for 1300 and 1550 nm. It thus would be of great interest to build an interrogation system for 800 nm range, offering advantages of low-cost and compact size. In this paper, we present a TFBG-based side detection spectrometer system with operational range around 800 nm, its application for measuring changes to strain and temperature experienced by FBGs, and its further implementation as a refractive index sensing system.

II. Principle and TFBGs Fabrication

A. Principle

When incident light in core modes composed of various wavelengths encounters a TFBG, it is radiated out of the fiber core in diverse directions with different strengths. The strongest light coupling only takes place when the phase match condition shown below is satisfied

$$\vec{K}_R = \vec{K}_C + \vec{K}_G \tag{1}$$

where $\vec{K}_R, \vec{K}_C$, and $\vec{K}_G$ are wave vectors of the radiation mode, the core mode, and the grating mode, respectively.

Further deduction from phase-match condition [9] yields the relation among the radiation angle (ξ) of the coupled light with certain wavelength (λ) in the radiation range of the TFBG, the period (Λ) of fringes in the fiber core and the tilted angle (θ) as follows:

$$\tan(\xi) = \frac{\lambda \sin(\theta)}{\lambda \cos(\theta) - n\Lambda} \tag{2}$$

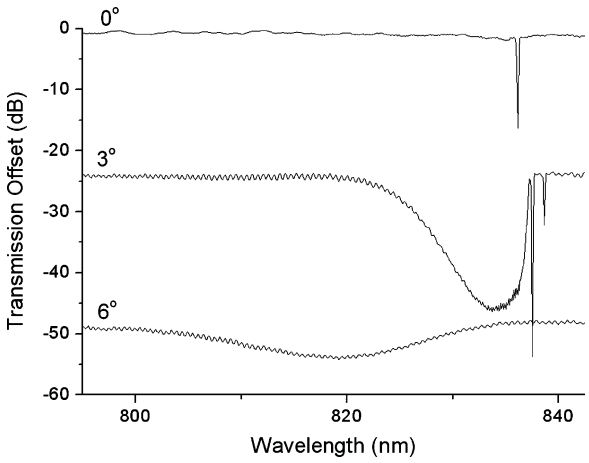

Fig. 2. The transmission spectra for FBG and TFBGs with 3° and 6° tilted angles fabricated using the same phase-mask.

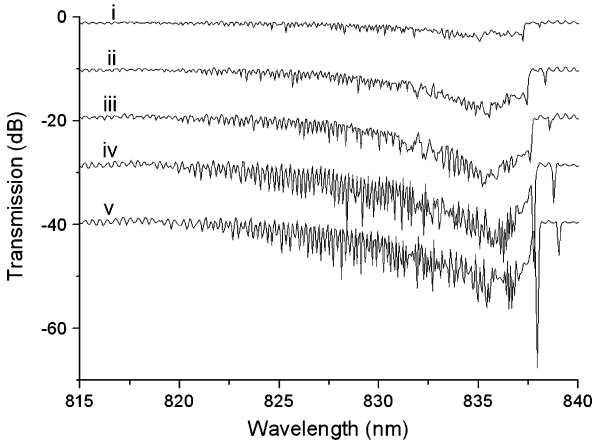

Fig. 3. The transmission spectra for a $3^{\circ}_{\rm ext}$-TFBG with different UV exposure time. Curve i–v present the spectra of TFBGs scanned by UV for 1–5 times.

where n is the refractive index of the fiber. (Since the refractive indices of the core and the cladding are very close, we take an average value in calculation.)

Owing to the cylindrical geometry of the fiber, the internal fringe angle (θ) is not the same as the tilted angle of the phase-mask $(\theta_{\rm ext})$. When the TFBG is fabricated using the phase-mask inscription method, the relationship between internal and external fringe angles is given by [10]

$$\theta = \frac{\pi}{2} - \tan^{-1}\left[\frac{1}{n\tan(\theta_{\rm ext})}\right] \tag{3}$$

B. TFBGs Fabrication

We have previously shown that the fringe angle of TFBGs in single-mode and multimode fiber, written by holographic and phase-mask fabrication technique, will directly affect both the strength and bandwidth of the out-coupled radiation profile for a given grating period [11]. In this experiment, TFBGs were UV-written in hydrogenated 820 nm single-mode fibers by phase-mask method. The period of the employed phase-mask was 0.5742 μm. Fig. 2 shows the transmission spectra of FBG and TFBGs with $3^{\circ}_{\rm ext}$ and $6^{\circ}_{\rm ext}$ tilted angles fabricated using the same phase-mask. From Fig. 2, it is observed clearly that the transmission-loss characteristics are related to the tilted angle. With the tilted angle increasing, the radiation-mode out-coupling (appearing as a broad transmission-loss profile) evolves as a result of blue shift of its central wavelength and increase in its dynamic range. It should be pointed out that in order to eliminate the resonant features in the transmission spectrum caused by the cladding-mode coupling effect, the gratings were immersed in index-matching gel to mimic an infinite cladding layer resulting in smooth radiation profiles, as shown in Fig. 2. It is noted that a very strong and narrow loss peak at the shorter wavelength side of the Bragg resonance occurred in the spectrum of $3^{\circ}_{\rm ext}$-TFBG, as shown in Figs. 2 and 3. This is a ghost mode, resulted from the coupling between the fundamental mode and backward $\rm LP_{1n}$ modes caused by the UV-induced asymmetrical index distribution in the fiber [12], [13].

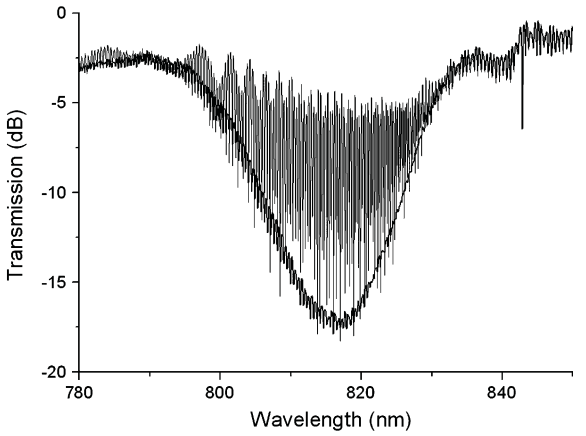

Fig. 4. Transmission spectrum of a $7^{\circ}_{\rm ext}$-TFBG. The comb-like resonances are measured with the TFBG in air; while the smooth curve is measured with the TFBG immersed in the index-matching gel.

Apart from the tilted angle, the transmission-loss characteristics of TFBGs are also related to the strength of index modulation. We have monitored the TFBG growth by scanning the UV beam across the fiber several times with the exposure length of 15 mm, UV power of 45 mW, and the scan speed of 0.07 mm/s. Fig. 3 shows the recorded transmission spectra for a $3^{\circ}_{\rm ext}$-TFBG after each scan. The profiles were measured without immersing gratings in the index-matching gel. We can see that with the exposure time increasing, more cladding modes are excited at the shorter wavelength side, while those at the longer wavelengths grow stronger, so the overall radiation-mode profile becomes broader, and at the same time the Bragg resonance shifts to the longer wavelength side.

A $7^{\circ}_{\rm ext}$-TFBG was selected to be used in our side detection experiment. The transmission spectrum of this TFBG is shown in Fig. 4, exhibiting a radiation-mode out-coupling profile ranging from 800 to 830 nm with the maximum spectral attenuation of 15 dB at the central wavelength of 818 nm. Based on (3), the theoretical internal tilted angle, θ is 10.1°. Fig. 5 displays the microscopic image of a $7^{\circ}_{\rm ext}$-TFBG, which clearly shows the slanted fringe features. We note that the fringe space is $\sim 0.574\ \mu$m, close to the phase-mask period, instead of a half of it. This is caused by the Talbot effect [14]. From Fig. 5, we

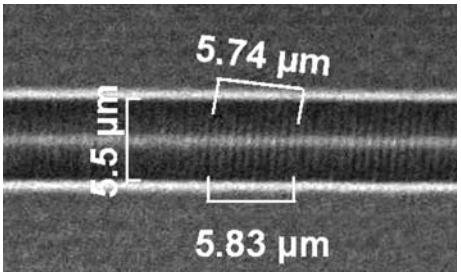

Fig. 5. Photo of a 7°_{ext}-TFBG UV-written in hydrogenated 820 nm single-mode fiber taken under the microscope.

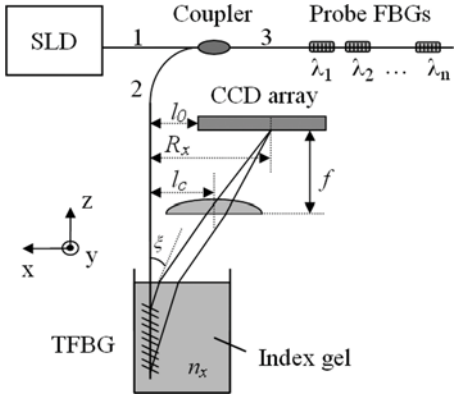

Fig. 6. Schematic diagram of the apparatus used for the TFBG-CCD interrogation system.

measured that the fringe spacing along the fiber axis is $0.583\mu\text{m}$. Thus, the internal fringe angle can be estimated as around 10.1°, which is in good agreement with the theoretical value. Deduction from (2), the radiation angle ξ is calculated as $\sim 20^{\circ}$ when the refractive index of the selected gel in the spectrum analyzer experiment is 1.4435.

III. 800 nm WDM Interrogation System

A. System Setup and Configuration

The experimental setup of the wavelength-division-multiplexing (WDM) interrogation system is shown in Fig. 6. A pigtailed super luminescent diode (SLD) with the central wavelength of 830 nm and the full optical bandwidth (wavelength range with output power above -40 dBm) of 60 nm was used as a broadband light source. The 7°_{ext}-TFBG used as the out-coupling device in this system was immersed in the index-matching gel to transfer the coupled light from the fiber cladding to the air. A SONY ILX511 linear CCD-array consisting of 2048 14 μm-pixels was positioned along x axis and mounted on a motorized translation stage to be moveable along y axis direction for scanning the radiation profile. A cylindrical lens was used to focus the light radiated from the TFBG to the CCD-array. The relative spectral sensitivity of the CCD-array to 400–1000 nm radiation given by the manufacturer is shown in Fig. 7.

Light from a broadband light source was fed to the FBG sensor via a 3 dB coupler. The reflected light from the FBG then propagated to the TFBG and part of the light was out-coupled into the surrounding gel by the TFBG.

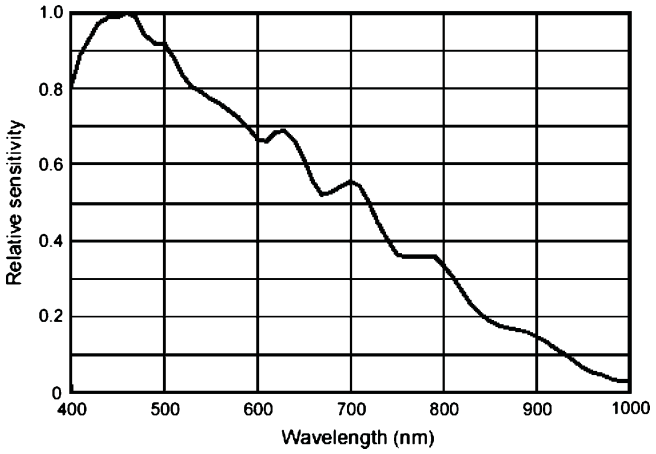

Fig. 7. The relative spectral sensitivity of the CCD-array to 400–1000 nm radiation.

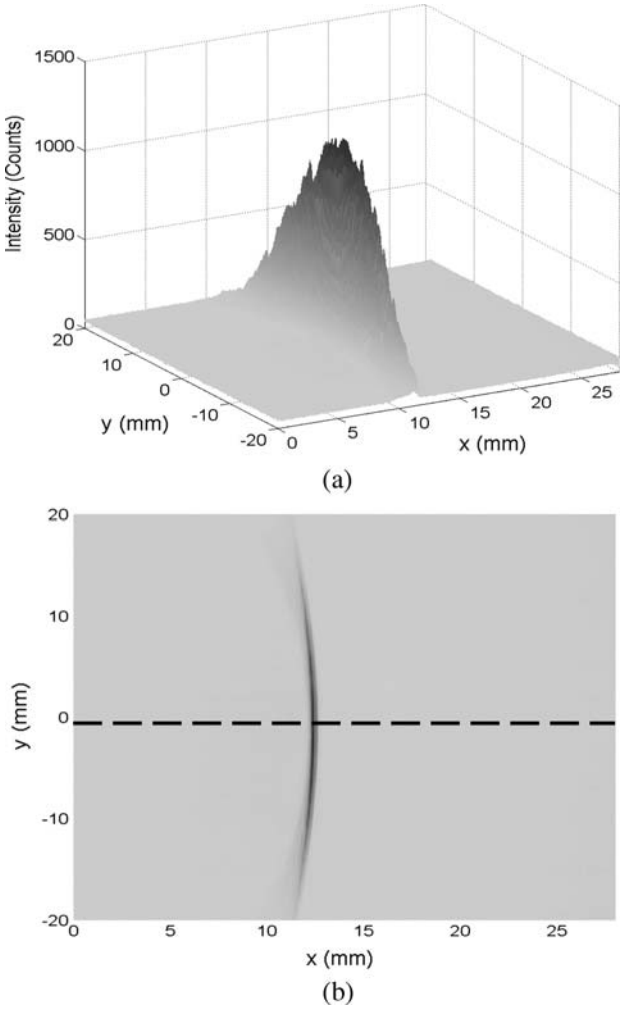

Fig. 8. Far-field image of radiated light captured by CCD-array. (a) 3-D-image. (b) Contour plot in x-y plane. The dash line in (b) indicating the center position where the TFBG radiated light is strongest.

Fig. 8(a) and (b) demonstrate a 3-D intensity plot and a contour plot in x-y plane of the radiated beam profile captured by CCD-array scanning along the y axis. The radiated beam is coupled outwards by the TFBG and focused by the cylindrical lens. With the real-time feedback of the CCD-array, the optics can be

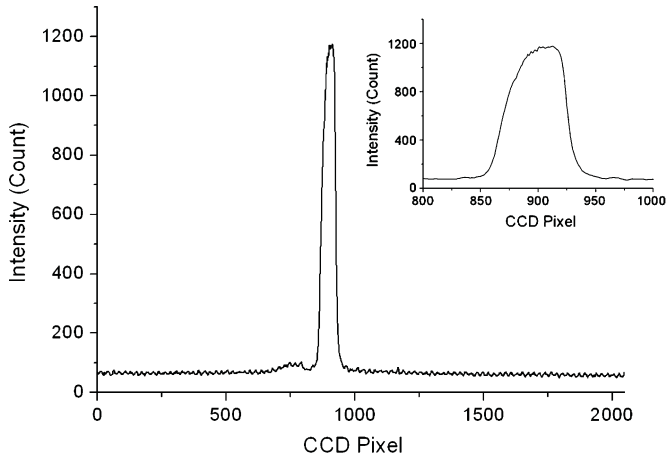

Fig. 9. Examples of radiation signal captured by CCD-array along the dashed line plotted from 0 to 2047 pixels. Inset: Zoomed signal plotted from 800 to 1000 pixels.

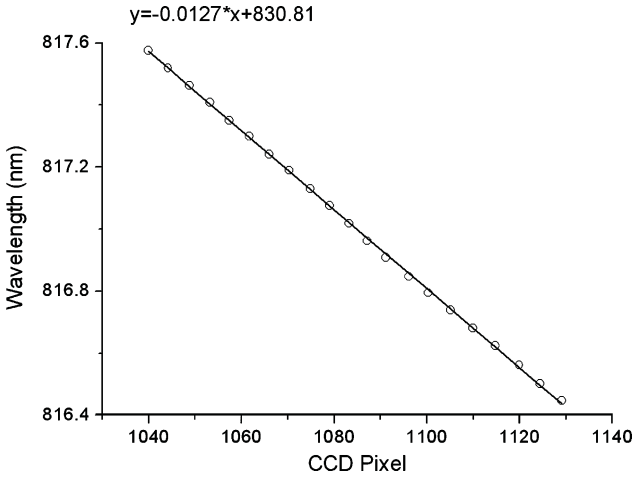

Fig. 10. Calibration plot of wavelength shift against CCD pixel.

aligned to achieve a symmetrical radiation pattern, as shown in Fig. 8(b). The movement of the pattern can be correlated and subsequently used to interrogate certain experimental factors such as the wavelength of the FBG and the refractive index of the surrounding gel, etc. Fig. 9 shows the reflection spectrum of an FBG captured when the CCD-array is positioned above the center of the radiated light [dashed line in Fig. 8(b)].

Pixilation is a simple consequence of the finite width ($14\ \mu\mathrm{m}$) of the pixels used in the CCD-array and represents the minimum physical resolution of the system. The inset of Fig. 9 shows the zoomed signal, from which we can hardly identify the central pixel of this signal. Therefore, a function is demanded to transfer the signal profiles to pixels. The centroid detection algorithm (CDA) was employed in our experiment to achieve this transformation and improve the system performance and resolution. CDA takes the amplitude weighted mean of the data according to (4) [15]

$$\widehat{i} = \frac{\sum_{1}^{2048} x_i \cdot y_i (> y_{\min})}{\sum_{1}^{2048} y_i} \tag{4}$$

where $\widehat{i}$ is the centroid fitted peak value, x_i is the wavelength of the i^{th} element, and $y_i(> y_{\min})$ is the amplitude of the i^{th} element greater than the noise floor $y_{\min}$.

B. Spectrum Analyzer Function

Since the interrogation system is based on the spectral-spatial encoding function of the TFBG-CCD structure, the correlation between the wavelength shift and the CCD pixel needs to be calibrated before measurement. The transfer function was obtained by implementing a strain sensing experiment. With tension applied on an FBG, its wavelength drifting was monitored by an optical spectrum analyzer (OSA) and our interrogation system at the same time. Fig. 10 shows the linear relationship between the Bragg wavelength and the CCD reading of this 800 nm-interrogation system using a lens of 155 mm focal length. The conversion coefficient is 12.7 pm/pixel, thus the spectral resolution of the system is 12.7 pm.

TABLE I
SYSTEM PARAMETERS SUMMARY FOR TWO LENSES

Focal length (mm)	Bandwidth (nm)	Gradient (nm/mm)	Spectral resolution (pm)
45	60	3.34	46.6
155	26	0.91	12.7

The bandwidth of the system is limited by the detection-length of the CCD-array, the focal length of the lens and the radiation range of the TFBG. With the given $7°_{\mathrm{ext}}$-TFBG and CCD-array, the bandwidth of the system is only determined by the focal length, which may be simply calculated by multiplying the spectral resolution and the number of pixels. The system parameters (bandwidth, spectral resolution) for two focal lengths are calculated, as shown in Table I.

Considering the radiation profile of the $7°_{\mathrm{ext}}$-TFBG from 800 to 830 nm and using the most length of the CCD-array, a cylindrical lens with a focal length of 155 mm was employed in the experimental system, therefore, the bandwidth and resolution of the system are 26 nm and 12.7 pm, respectively.

Fig. 11(a) shows the spectral shifts of a sensing FBG with a Bragg resonance at 816.5 nm measured by the TFBG-CCD interrogation system when the strain on the grating increased from 0 to 1904.8 $\mu\varepsilon$, while Fig. 11(b) shows the results of the same FBG measured when the temperature changed from 0 °C to 60 °C with a step of 2 °C. From Fig. 11(a) and (b), the strain and temperature sensitivities are estimated as 0.59 $\mathrm{pm}/\mu\varepsilon$ and 5.6 $\mathrm{pm}/°\mathrm{C}$, respectively, which are in good agreement with the reported typical results of 0.64 $\mathrm{pm}/\mu\varepsilon$ and 6.8 $\mathrm{pm}/°\mathrm{C}$ near the wavelength of 830 nm [16]. The points marked with "O" in Fig. 11 represent the shifts in the Bragg wavelength calculated by the CDA, while those marked with "X" are the values calculated simply on maximum points of the signals. It is clear that the CDA improves the system performance significantly.

Fig. 12(a) shows the wavelength drifts recorded over a period of 45 min. The regular fluctuation pattern may be induced by the perturbation of room temperature. Fig. 12(b) shows a histogram displaying the distribution of the spectral drifts that clearly forms a normal distribution. The root mean square (RMS) deviation from the mean of this histogram is merely 1.6 pm, which indicates that the system is inherently stable.

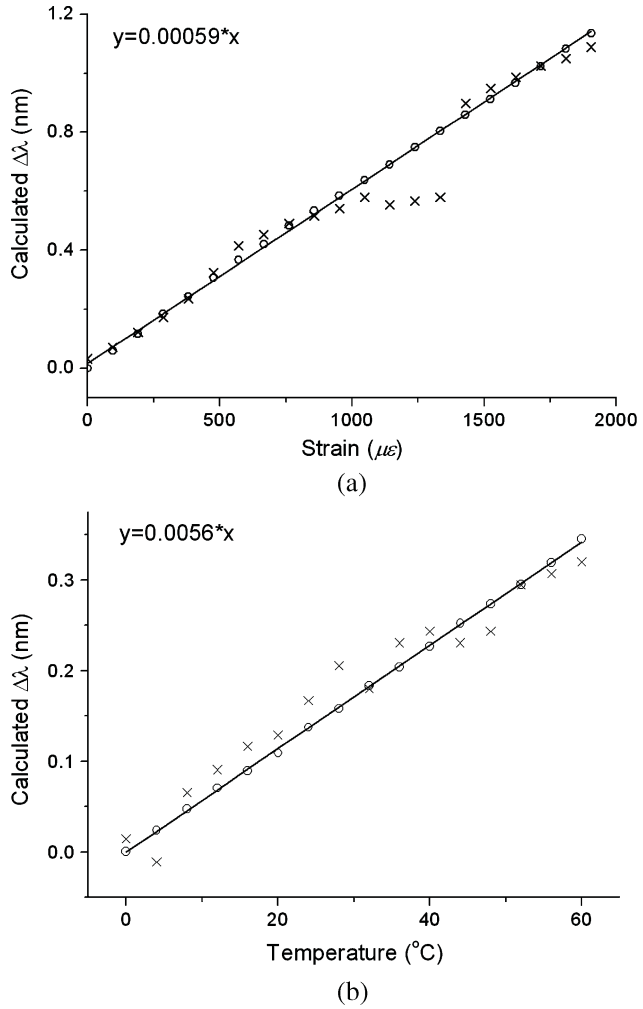

Fig. 11. Spectral shift measured by the interrogation system against: (a) strain and (b) temperature on sensing FBG. In both (a) and (b), the points marked with "O" are the data obtained by CDA; while those marked with "X" are simply given by maximum reading method.

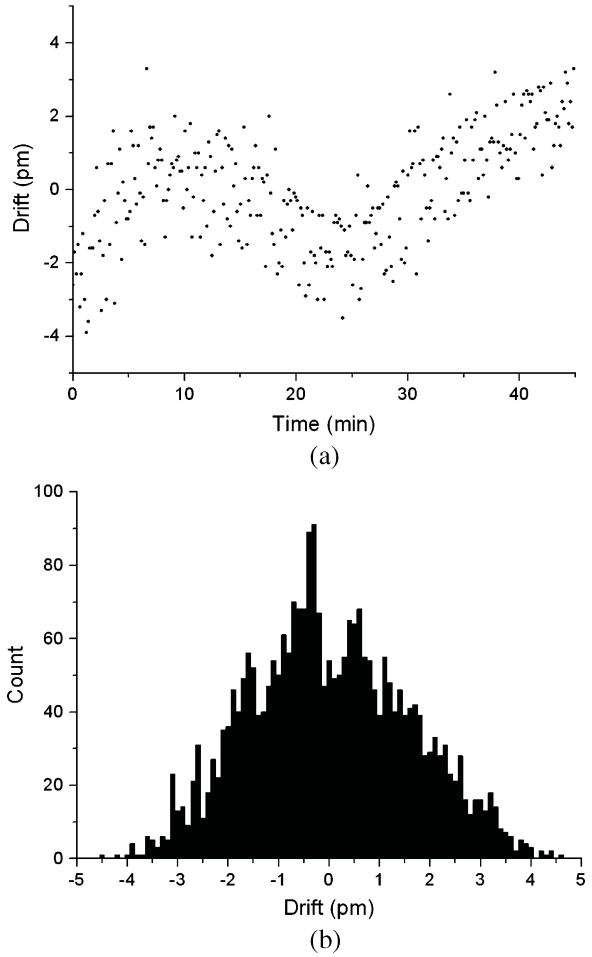

Fig. 12. Spectral drifts over time of the sensing FBG measured with the TFBG-CCD system: (a) Wavelength shifts of λ against time. (b) Histogram to show the distribution of the spectral drifts over a 45-min period.

Although we only demonstrated the measurement to one FBG sensor, this TFBG-CCD interrogation system should be capable of performing WDM interrogation detecting multiple signals within its dynamic range.

C. Refractive Index Sensing Function

With a fixed probe light, the system can also be applied to measure the surrounding-medium refractive index (SRI) of the TFBG. Thus, the above described spectrum analyzer system has the capability of detecting bio/chemical samples, which may have a potential use for medicine, environmental monitoring and life science applications.

As shown in Fig. 6, the reflection of the FBG propagates to the TFBG, a section of which is out-coupled to the surrounding gel by the TFBG with a radiation angle ξ. With the given 7°_{ext}-TFBG, the distance from the fiber to the focal point along x axis, R_x (named as radiation radius), is related to the refractive index of the liquid n_x as follows:

$$R_x = l_c + f\sqrt{\frac{n_x^2 - n^2\cos^2(\xi)}{1 - n_x^2 + n^2\cos^2(\xi)}} \tag{5}$$

where l_c represents the distance between the fiber and the center of the lens along x axis, f is the focal length, and n is the refractive index of the fiber.

With a selected position in the CCD-array, we can also derive the relationship between the CCD pixel and refractive index as

$$N_x = (R_x - l_0)/0.014 \tag{6}$$

where l_0 is the position of the first (No. 0) pixel in the CCD-array indicated in Fig. 6, and 0.014 is the length of one CCD pixel in mm.

From (5), we can derive that the refractive index of the sample liquid n_x is limited as

$$n\cos(\xi) < n_x < \sqrt{1 + n^2\cos^2(\xi)}. \tag{7}$$

Substituting the system parameters: ξ and n, the measurable SRI range n_x is from 1.362 to 1.689.

In the experiment, we employed glycerin with the refractive index of 1.4735 as sample liquid, which is soluble in water in any mixing ratio. The glycerin solution can be produced with the refractive index from 1.3333 to 1.4735, which provides a good dynamic range for the SRI experiment.

TABLE II
THE RADIATION RADII USING DIFFERENT LENSES

n_x	1.3712	1.3848	1.3988	1.4132
R_x (mm) f=45mm	31.52	35.82	39.29	42.46
R_x (mm) f=155mm	49.90	64.72	76.66	87.58
n_x	1.4280	1.4432	1.4589	1.4735
R_x (mm) f=45mm	45.52	48.57	51.74	54.74
R_x (mm) f=155mm	98.13	108.70	119.56	129.89

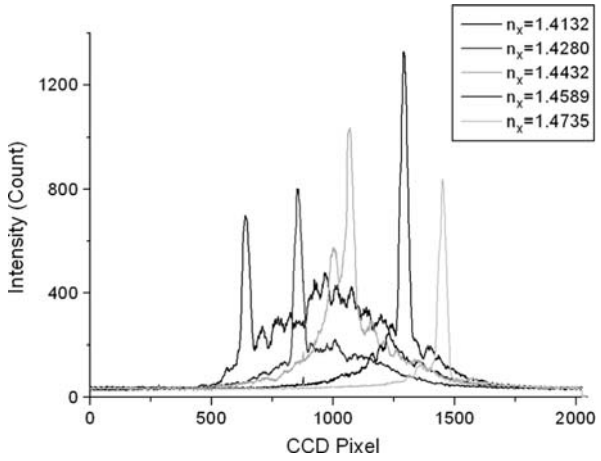

Fig. 13. The signals detected by CCD-array using different glycerin solutions.

Similar to the system function discussed above, the dynamic range here is also limited by the focal length and the size of the detecting area of the CCD-array. Substituting the system parameters: $l_c = 24\,\mathrm{mm}, n = 1.446$ and considering a common SRI range from 1.3712 to 1.4735, the radiation radius, R_x, can be calculated according to (5). Table II lists the calculated values of R_x for two focal lengths: 45 and 155 mm.

When the refractive index of the sample liquid varies, the radiation beam illuminates the CCD-array at the different position. Therefore, the refractive index of the sample liquid can be decoded from the CCD signals.

Considering the detection-length of CCD-array is 28 mm, from Table II, we can see that with given $l_0 \sim 33\ \mathrm{mm}$ and for SRI range from 1.3712 to 1.4735, a lens of 45 mm focal length is more suitable for using most CCD-array detection area. However, as shown in Fig. 6, the SRI measurement range can also be limited by the size of the cylindrical lens. During our experiment, it has been recognized that light will not be collected and focused effectively by the cylindrical lens when the refractive index of the liquid is below 1.4. Fig. 13 shows the signals detected by the CCD-array using different sample liquids with SRIs above 1.4 at the same fluid level.

Based on (5), we theoretically simulated the relationship between the radiation radius R_x and the refractive index of sample liquid n_x in the range of n_x from 1.362 to 1.689, as shown in Fig. 14. Overall, the relation is nonlinear, especially when n_x is close to 1.689, however, it is nearly linear from 1.41 to 1.48.

Considering the length of the CCD-array and the size of the cylindrical lens, we selected the sample liquids with refractive indices in the almost linear range (1.41∼1.48) of the simulation curve in Fig. 14. The refractive indices of sample liquid n_x used in the experiment varied from 1.4132 to 1.4735. Fig. 15 plots

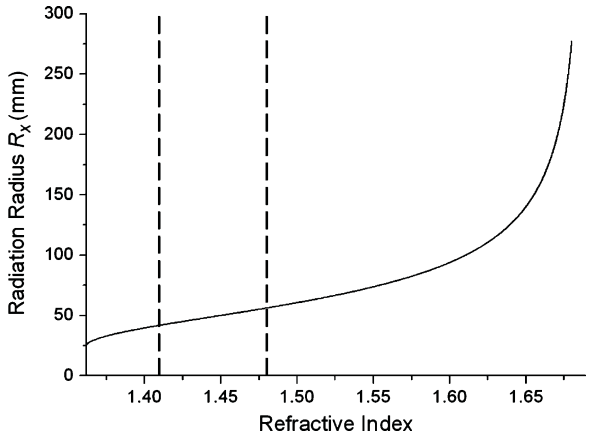

Fig. 14. The theoretical simulation plot of the radiation radius R_x against the refractive index of sample liquid n_x in the range from 1.362 to 1.689.

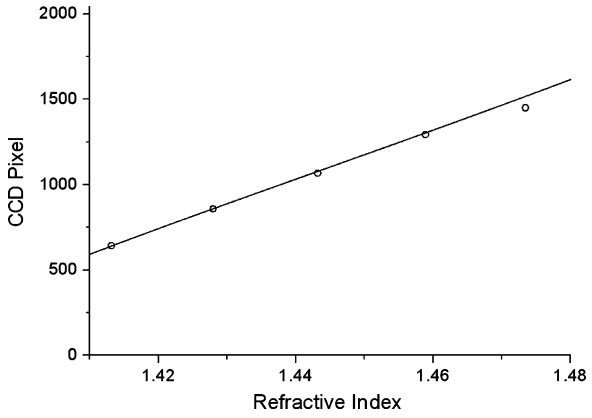

Fig. 15. CCD pixel shift against refractive index change in the range from 1.41 to 1.48.

the correlation between SRI and CCD pixels, showing a near-linear response. Since a single pixel of CCD-array can be readily resolved, from the plot we can estimate that the SRI change as small as 10^{-5} should be detectable by this system.

IV. CONCLUSION

We have demonstrated a TFBG-based 800 nm WDM interrogation system, which can function as an in-fiber spectrum analyzer with an interrogation bandwidth up to 60 nm and a resolution of 12.7 pm. The system was evaluated by performing the FBG strain and temperature sensing experiments, obtaining the strain and temperature sensitivities of 0.59 $\mathrm{pm}/\mu\varepsilon$ and 5.6 $\mathrm{pm}/^{\circ}\mathrm{C}$, which are in good agreement with the reported typical values. In addition, the system was further evaluated for sensing the refractive index of sample liquids. In the near-linear range from 1.4132 to 1.4735, we estimate that the SRI change as small as 10^{-5} can be detected by this low-cost high-resolution TFBG WDM interrogation system.

REFERENCES

[1] A. D. Kersey *et al.*, "Fiber grating sensors," *J. Lightw. Technol.*, vol. 15, pp. 1442–1463, 1997.

[2] G. Meltz, W. W. Morey, and W. Glenn, "In-fiber Bragg grating tap," presented at the Optical Fiber Commun. Conf., Washington, DC, 1990, TuG1, Optical Society of America, unpublished.

[3] G. Meltz, W. W. Morey, and A. Wilson, "Optical waveguide embedded light redirecting and focusing Bragg grating arrangement," U.S., 1991.
[4] K. S. Feder, P. S. Westbrook, J. Ging, P. I. Reyes, and G. E. Carver, "In-fiber spectrometer using tilted fiber gratings," *Photonics Technol. Lett.*, vol. 15, pp. 933–935, 2003.
[5] C. Jauregui and J. Lopez-Higuera, "Interrogation of fiber Bragg gratings with a tilted fiber Bragg grating," *Meas. Sci. Technol.*, vol. 15, pp. 1596–1600, 2004.
[6] J. L. Wagener, T. A. Strasser, J. R. Pedrazzani, J. Demarco, and D. J. Digiovanni, "Fiber grating optical spectrum analyzer tap," in *Proc. ECOC '97*, 1997, pp. 65–68.
[7] S. Wielandy and S. C. Dunn, "Tilted superstructure fiber grating used as a Fourier-transform spectrometer," *Opt. Lett.*, vol. 29, no. 14, pp. 1614–1616, 2004.
[8] A. G. Simpson, K. Zhou, L. Zhang, L. Everall, and I. Bennion, "Optical sensor interrogation with a blazed fiber Bragg grating and a charge-coupled device linear array," *Appl. Opt.*, vol. 43, pp. 33–40, 2004.
[9] K. Zhou, L. Zhang, X. Chen, and I. Bennion, "Low thermal sensitivity grating devices based on ex-45 ° tilting structure capable of forward-propagating cladding modes coupling," *J. Lightw. Technol.*, vol. 24, no. 12, pp. 5087–5094, 2006.
[10] R. W. S. J. Mihailov, P. Lu, H. Ding, X. Dai, C. Smelser, and L. Chen, "UV-Induced polarisation-dependant loss (PDL) in tilted fiber Bragg gratings: Application of a PDL equaliser," *IEE Proc. Optoelectronics*, vol. 149, p. 211, 2002.
[11] K. Zhou, A. G. Simpson, L. Zhang, and I. Bennion, "Side detection of strong radiation mode out-coupling from blazed FBGs in single- and multi-mode fibers," *Photon. Technol. Lett.*, vol. 15, pp. 936–938, 2003.
[12] W. W. Morey, G. Meltz, J. D. Love, and S. J. Hewlett, "Mode-coupling characteristics of UV-written Bragg gratings in depressed-cladding fiber," *Elec. Lett.*, vol. 30, pp. 730–732, 1994.
[13] S. J. Hewlett, J. D. Love, G. Meltz, T. J. Bailey, and W. W. Morey, "Coupling characteristics of photo-induced Bragg gratings in depressed- and matched-cladding fiber," *Opt. Quantum Electron.*, vol. 28, pp. 1641–1654, 1996.
[14] N. M. Dragomir, C. Rollinson, S. A. Wade, A. J. Stevenson, S. F. Collins, G. W. Baxter, P. M. Farrell, and A. Roberts, "Nondestructive imaging of a type I optical fiber Bragg grating," *Opt. Lett.*, vol. 28, pp. 789–791, 2003.
[15] A. Ezbiri, S. E. Kanellopoulos, and V. A. Handerek, "High resolution instrumentation system for fiber-Bragg grating aerospace sensors," *Opt. Commun.*, vol. 150, pp. 43–48, 1998.
[16] Y. J. Rao, "In-fiber Bragg grating sensors," *Meas. Sci. Technol.*, vol. 8, pp. 355–375, 1997.

Rui Suo received the M.Sc. degree in optical engineering from Tsinghua University, Beijing, China, in 2005. He is currently working towards the Ph.D. degree at Aston University, Birmingham, U.K.

His current research interest is in the field of fiber grating technology and its applications in telecommunications and optical sensing.

Xianfeng Chen received the M.S. degree in optics from Suzhou University, China, in 2001 and the Ph.D. degree in electronic engineering from Aston University, Birmingham, U.K., in 2006.

He is currently working as a Research Fellow at Aston University in the field of fiber grating technology and its applications in telecommunications and optical sensing, biophotonics, and fiber lasers. He has published more than 60 journal and conference papers.

Kaiming Zhou received the B.S. and M.S. degrees in physics from Nankai University, Tianjin, China, in 1993 and 1996, respectively, and the Ph.D. degree from the Institute of Semiconductor, Chinese Academy of Sciences, Beijing, in 1999, where he spent another two years as a Postdoc supervising a project on external cavity semiconductor lasers with fiber Bragg grating as cavity mirror.

In 2002, he joined the Photonics Research Group, Department of Electronic Engineering, Aston University, Birmingham, U.K., and has been investigating optical properties and applications of tilted fiber Bragg grating. His current research interest is in the field of fiber grating technology and its applications in telecommunications and optical sensing, biosensor, biophotonics. He has authored and coauthored over 50 journal and conference papers.

Dr. Zhou is a member of Optical Society of America (OSA).

Lin Zhang received the Ph.D. degree in physics in 1990 from the University of Sussex, Sussex, U.K.

She then, she worked as a Research Fellow at the University of Sussex, in the area of active and passive planar waveguide devices. She joined the Photonics Research Group, School of Engineering and Applied Science, Aston University, Birmingham, U.K., in 1994. Since then, she has been researching mainly in the field of fiber grating technologies and applications, and extensively involved in a number of LINK, EPSRC, EU, and DERA funded research programs. She has authored and coauthored over 350 international standard journal and conference papers and two books. Her research interests include fiber and guidewave optics and devices, interferometric optics, fiber grating devices, optical sensors and sensing technologies, UV and femtosecond inscription techniques and photosensitivity, and biophotonics.

Ian Bennion (M'91) has been a Professor of Photonics at the School of Engineering and Applied Science since joining Aston University, Birmingham, U.K., as Co-founder of the Photonics Research Group in September 1991. He is presently leader of the group and head of the Electronic Engineering Subject Group. Previously, he spent 16 years at Plessey Research Caswell, Ltd., latterly GEC-Marconi Materials Technology, Ltd., researching optoelectronic devices and their applications. His most recent research activities have been in the fields of fiber grating technology and its applications, optical sensor technology, biophotonics, high-speed fiber-optic communications, and fiber-optic signal processing. He has published more than 500 journal and conference papers on photonics.

He is a Fellow of the IEE and of the Institute of Physics (U.K.), and a Member of the Optical Society of America and of the IEEE.